Multiscale Modeling and Computation of Incompressible Flow *

Thomas Y. Hou†

Abstract. Many problems of fundamental and practical importance contain multiple scale solutions. Composite materials, flow and transport in porous media, and turbulent flow are examples of this type. Direct numerical simulations of these multiscale problems are extremely difficult due to the range of length scales in the underlying physical problems. In this paper, we review the multiscale finite element method introduced in [27, 28] and describe some of its applications, including flow and transport in heterogeneous porous media. An important feature of the multiscale finite element method is that it can be applied to problems with many or continuous spectrum of scales without scale separation. Further, we introduce a new multiscale analysis for convection dominated 3-D incompressible flow with multiscale solutions. The main idea is to construct semi-analytic multiscale solutions locally in space and time, and use them to construct the coarse grid approximation to the global multiscale solution. Such approach overcomes the common difficulty associated with the memory effect and the non-uniqueness in deriving the effective equations for incompressible flows with multiscale solutions. Our multiscale analysis provides an important guideline in designing a systematic multiscale method for computing incompressible Euler and Navier-Stokes flow with multiscale solutions.

1 Introduction

Many problems of fundamental and practical importance have multiple scale solutions. Composite materials, wave propagation in random media, flow and transport through heterogeneous porous media, and turbulent flow are examples of this type.

*Research was in part supported by the National Science Foundation through a grant DMS-0073916 and an ITR grant ACI-0204932.

†Applied Mathematics, 217-50, Caltech, Pasadena, CA 91125, USA. Email: hou@ama.caltech.edu

The direct numerical solution of multiple scale problems is difficult due to the wide range of scales in the solution. It is almost impossible to resolve all the small scale features by direct numerical simulations due to the limited capacity in computing power. On the other hand, from an engineering perspective, it is often sufficient to predict the macroscopic properties of the multiscale systems, such as the effective conductivity, elastic moduli, permeability, and eddy diffusivity. Therefore, it is desirable to develop a coarse grid method that captures the small scale effect on the large scales, but does not require resolving all the small scale features.

In recent years, we have introduced a multiscale finite element method (MsFEM) for solving partial differential equations with multiscale solutions [27, 28, 20, 9]. The central goal of this approach is to obtain the large scale solutions accurately and efficiently without resolving the small scale details. The main idea is to construct finite element base functions which capture the small scale information within each element. The small scale information is then brought to the large scales through the coupling of the global stiffness matrix. Thus, the effect of small scales on the large scales is captured correctly. In our method, the base functions are constructed from the leading order differential operator of the governing equation within each element. This leading order operator is typically an elliptic operator with highly oscillatory coefficients for composite materials, flow in porous media, wave propagation in random media, or convection dominated transport with multiscale velocity field. As a consequence, the base functions are adapted to the local microstructure of the differential operator. In the case of two-scale periodic structures, we have proved that the multiscale method indeed converges to the correct solution independent of the small scale in the homogenization limit [28, 20, 9].

One of the main difficulties in deriving effective multiscale methods is to derive accurate *local* microscopic boundary conditions that connect small scale solution from one coarse grid block to the neighboring coarse grid blocks. If one naively imposes a smooth boundary condition for multiscale bases at the boundary of a coarse grid element, it will create a mismatch between the global multiscale solution and the approximate solution constructed by the multiscale numerical method. Using homogenization theory, we have identified a resonance error which manifests as the ratio between the physical small scale and the coarse grid mesh size [27, 20]. Our analysis indicates that if we use inappropriate microscopic boundary conditions for the multiscale bases, it will generate a boundary layer in the boundary corrector of the multiscale base, which seems to be responsible for generating the resonance error. In the case when the coefficient has scale separation and periodic structure, we can solve the periodic cell problem to construct the "ideal" microscopic boundary condition which eliminates the artificial boundary layer in the boundary corrector. In this special case, we also obtain an analytic formulation for the multiscale bases. However, this approach can not be generalized to problems with many or continuous spectrum of scales. On the other hand, our analysis indicates that interactions of small scales are strongly localized for elliptic or parabolic problems. Motivated by this observation, we propose an over-sampling technique which can effectively reduce the resonance error [27]. The over-sampling technique is quite general and can be applied to problems with many or continuous spectrum of scales.

We have applied the multiscale finite element method with the over-sampling

technique to several applications, ranging from problems in composite material, to wave propagation in random media, convection dominated transport, and two-phase flow in heterogeneous porous media. The agreements between the coarse grid multiscale finite element calculations and the corresponding well-resolved calculations are striking. We remark that from practical application view point, it is important that multiscale computational methods can be applied to problems with an infinite number of scales that are not separable. In many applications, such as transport of flow through heterogeneous porous media, the multiscale coefficient such as permeability tensor has a continuous spectrum of scales without scale separation or periodic structure. Therefore it is essential that we do not make explicit use of the assumption on scale separation and periodic structure in our multiscale finite element method.

We remark that the idea of using base functions governed by the differential equations has been used in the finite element community, see e.g. [3]. In particular, the multiscale finite element method is similar in spirit to the residual-free bubble finite element method [6, 44] and the variational multiscale method [33, 7]. There are also other multiscale methods that explore homogenization theory or separation of scales to derive effective coarse grid methods, see e.g. [13, 37, 38, 24, 8, 10, 21].

While a lot of progress has been made in developing multiscale methods to solve elliptic or diffusion dominated problems, there is only limited success in developing effective multiscale methods for convection dominated transport in heterogeneous media [39, 17, 35, 48, 19, 31]. One of the common difficulties for this problem is the so-called nonlocal memory effect [46]. For nonlinear convection problems, it is also difficult to characterize how small scales propagate in time and what kind of small scale structures is preserved by the flow dynamically.

Recently, together with Dr. Danping Yang [30, 32], we have developed a systematic multiscale analysis for the 3-D incompressible Euler equations with highly oscillating initial velocity field. The understanding of scale interactions for 3-D incompressible Euler and Navier-Stokes equations have been a major challenge. For high Reynolds number flows, the degrees of freedom are so high that it is almost impossible to resolve all small scales by direct numerical simulations. Deriving an effective equation for the large scale solution is very useful in engineering applications. The nonlinear and nonlocal nature of the incompressible Euler or Navier-Stokes equations makes it difficult to construct a properly-posed multiscale solution.

The key idea in constructing our multiscale solution for the Euler equation is to reformulate the problem using a new phase variable to characterize the propagation of small scales. This phase variable is essentially the backward flow map. The multiscale structure of the solution becomes apparent in terms of this phase variable. Our analysis is strongly motivated by the pioneering work of McLaughlin-Papanicolaou-Pironneau (MPP for short) [39]. The main difference is that MPP assumed that the small scales are convected by the mean flow, while we believe that the small scales are convected by the full velocity field. In fact, by using a Lagrangian description of the Euler equation, we can see that small scales are indeed propagated by the Lagrangian flow map. By using a Lagrangian description, we can characterize the nonlinear convection of small scales exactly and turn a convection dominated transport problem into an elliptic problem for the stream

function. Thus, traditional homogenization result for elliptic problems can be used to obtain a multiscale expansion for the stream function. At the end, we derive a coupled multiscale system for the flow map and the stream function. In order for the homogenized system to be well-posed, we need to impose a solvability condition, which is to ensure that there is no secular growth term in the first order correction of the flow map. The solvability condition can be interpreted as a projection or filtering to remove the resonant velocity component. Such resonant velocity component prevents the flow from fully mixing and can lead to the development of the nonlocal memory effect [46].

For computational purpose, it is more convenient to derive a homogenized equation in the Eulerian formulation. By using the key observation from our multiscale analysis in the Lagrangian formulation, we derive a well-posed homogenized equation in the velocity-pressure formulation. In our multiscale analysis in the Eulerian frame, we use the phase variable to describe the propagation of small scales in the velocity field, but use the Eulerian variable to describe the large scale solution. Since we treat the convection of small scales exactly by the phase variable, there is no convection term in the cell problem for the small scale velocity field. As a consequence, we can solve for the cell problem with a relatively large time step. Moreover, for fully mixed flow, we expect that the small scale solution would reach a statistical equilibrium relatively fast in time. In this case, we may need only to compute a small number of time steps in the cell problem to evaluate the Reynolds stress term in the homogenized equation for the averaged velocity. Moreover, we may express the Reynolds stress term as the product of an eddy diffusivity and the deformation tensor of the averaged velocity field, see e.g. [45, 36, 12, 25]. For fully mixed homogeneous flow, the eddy diffusivity is close to be a constant in space. In this case, we need only to solve one representative cell problem and use the solution of this representative cell problem to evaluate the eddy diffusivity. This would give a self-consistent coarse grid model that couples the evolution of the small and large scales dynamically.

The rest of the paper is organized as follows. In Section 2, we review the multiscale finite element method, describe the issue of microscopic boundary conditions for the multiscale bases. We then introduce the over-sampling technique and discuss the convergence property of the method. In Section 3, we present several applications of the multiscale finite element methods, including wave propagation in periodic and random media, convection enhanced diffusion, flow and transport in heterogeneous porous media. We also discuss how to use our multiscale method to upscale one-phase and two-phase flow. In Section 4, we describe some recent work in deriving nonlinear homogenization for the 3-D incompressible Euler equation.

2 Multiscale Finite Element Method

In this section, we briefly review the multiscale finite element method which was introduced in [27, 28] and has been applied to compute elliptic problems with highly oscillating coefficient, wave propagation in multiscale media, convection enhanced diffusion, transport of flow in strongly heterogeneous porous media. The multiscale

finite element method (MsFEM for short) is designed to effectively capture the large scale behavior of the solution without resolving all the small scale features. The main idea of our multiple scale finite element method consists of construction of finite element base functions which contain the small scale information within each coarse grid element. The small scale information is then brought into the large scales through the coupling of the global stiffness matrix.

It should be noted that MsFEM is different from the traditional domain decomposition method in an essential way, although the two methods appear to be similar. First of all, the design purposes are different. MsFEM is used as a method to obtain the correct discretization of the large scale problem on a relatively coarse grid, while the domain decomposition is an iterative method for solving the problem on a fine grid which resolves the small scales. One of the key features of MsFEM is that the construction of the base functions is a *local* operation within the coarse grid elements. Thus, the construction of the base function in one element is *decoupled* from that in another element. In contrast, in domain decomposition methods, the decomposed subdomains are still coupled together.

The decoupled construction of the multiple scale bases provides some advantages in the computation. First, the construction can be carried out perfectly in parallel. In effect, we break a large scale computation into many smaller and *independent* pieces. Thus, the method is automatically adapted to parallel computers. In addition, there is a great advantage in computer memory usage. Once the small scale information within an element is gathered into the global stiffness matrix, the memory used for those base functions can be reused to construct bases of the next element. Thus, we can sequentially sample a large amount of fine scale information from many elements with limited memory. Therefore, MsFEM is less constrained by the limit of computer memory than the direct methods. Another important feature of this approach is that small scale solutions can be reconstructed *locally* from the coarse grid computation by using the multiscale bases as interpolation bases. This feature is especially useful when we try to upscale two-phase flow in heterogeneous media. Moreover, by constructing the multiscale bases adaptively in space and time, we can recover the fine scale detail using only a fraction of time that is required for a direct fine grid simulation.

2.1 MsFEM for elliptic problems with oscillating coefficients

We will use the elliptic problem with highly oscillating coefficients as an example to illustrate the main idea of MsFEM. We consider the following elliptic problem:

$$L_\epsilon u := -\nabla \cdot (a^\epsilon(\mathbf{x})\nabla u) = f \quad \text{in } \Omega, \quad u = 0 \quad \text{on } \partial\Omega, \tag{1}$$

where $a^\epsilon(\mathbf{x}) = (a^\epsilon_{ij}(\mathbf{x}))$ is a positive definite matrix. This model equation represents a common difficulty shared by several physical problems. For flow in porous media, it is the pressure equation through Darcy's law. The coefficient a^ε represents the permeability tensor. For composite materials, it is the steady heat conduction equation and the coefficient a^ε represents the thermal conductivity. For steady transport problems with divergence-free velocity field, it is a symmetrized form of

the governing equation. In this case, the coefficient a_ε is a combination of transport velocity and viscosity tensor.

To simplify the presentation of the finite element formulation, we assume the domain is an unit square $\Omega = (0,1) \times (0,1)$. The variational problem of (1) is to seek $u \in H_0^1(\Omega)$ such that

$$a(u,v) = f(v), \qquad \forall v \in H_0^1(\Omega), \tag{2}$$

where

$$a(u,v) = \int_\Omega a_{ij}^\epsilon \frac{\partial v}{\partial x_i}\frac{\partial u}{\partial x_j} d\mathbf{x} \quad \text{and} \quad f(v) = \int_\Omega f v d\mathbf{x},$$

where we have used the Einstein summation notation. A finite element method is obtained by restricting the weak formulation (2) to a finite dimensional subspace of $H_0^1(\Omega)$. For $0 < h \leq 1$, let $\mathcal{K}^h$ be a partition of Ω by a collection of rectangles K with diameter $\leq h$, which is defined by an axi-parallel rectangular mesh. In each element $K \in \mathcal{K}^h$, we define a set of nodal basis $\{\phi_K^i, i = 1, \ldots, d\}$ with d being the number of nodes of the element. The subscript K will be neglected when bases in one element are considered. In our multiscale finite element method, ϕ^i satisfies

$$L_\epsilon \phi^i = 0 \qquad \text{in } K \in \mathcal{K}^h. \tag{3}$$

Let $\mathbf{x}_j \in \overline{K}$ $(j = 1, \ldots, d)$ be the nodal points of K. As usual, we require $\phi^i(\mathbf{x}_j) = \delta_{ij}$. One needs to specify the boundary condition of ϕ^i to make (3) a well-posed problem (see below). For now, we assume that the base functions are continuous across the boundaries of the elements, so that

$$V^h = \text{span}\{\phi_K^i : i = 1, \ldots, d; K \in \mathcal{K}^h\} \subset H_0^1(\Omega).$$

In the following, we study the approximate solution of (2) in V^h, i.e., to find $u^h \in V^h$ such that

$$a(u^h, v) = f(v), \qquad \forall v \in V^h. \tag{4}$$

Note that this formulation of the multiscale method is not restricted to the rectangular elements. It can also be applied to triangular elements which are more flexible in modeling complicated geometries.

2.2 Microscopic boundary conditions for multiscale bases

The choice of boundary conditions in defining the multiscale bases will play a crucial role in approximating the multiscale solution. Intuitively, the boundary condition for the multiscale base function should reflect the multiscale oscillation of the solution u across the boundary of the coarse grid element. To gain insight, we first consider the special case of periodic homogenization, i.e. when $a^\epsilon(\mathbf{x}) = a(\mathbf{x}, \mathbf{x}/\epsilon)$, with $a(\mathbf{x}, \mathbf{y})$ being periodic in $\mathbf{y}$. Using standard homogenization theory [4], we can perform multiscale expansion for the base function, ϕ^ϵ, as follows ($\mathbf{y} = \mathbf{x}/\epsilon$):

$$\phi^\epsilon = \phi_0(\mathbf{x}) + \epsilon\phi_1(\mathbf{x}, \mathbf{y}) + \epsilon\theta^\epsilon(\mathbf{x}) + O(\epsilon^2)\,,$$

where ϕ_0 is the effective solution, ϕ_1 is the first order corrector. The boundary corrector θ^ϵ is chosen so that the boundary condition of ϕ^ϵ on ∂K is exactly satisfied.

By solving a periodic cell problem for χ^j,

$$\nabla_{\mathbf{y}} \cdot a(\mathbf{x},\mathbf{y}) \nabla_{\mathbf{y}} \chi^j = \frac{\partial}{\partial y_i} a_{ij}(\mathbf{x},\mathbf{y}) \tag{5}$$

with zero mean, we can express the first order corrector ϕ_1 as follows: $\phi_1(\mathbf{x},\mathbf{y}) = -\chi^j \frac{\partial \phi_0}{\partial x_j}$. The boundary corrector, θ^ϵ, then satisfies

$$\nabla_{\mathbf{x}} \cdot a(\mathbf{x},\mathbf{x}/\epsilon) \nabla_{\mathbf{x}} \theta^\epsilon = 0 \quad \text{in} \quad K$$

with boundary condition

$$\epsilon\theta^\epsilon|_{\partial K} = (\phi^\epsilon - (\phi_0 + \epsilon\phi_1(\mathbf{x},\mathbf{x}/\epsilon))\,|_{\partial K} \ .$$

In general, the boundary condition of θ^ϵ has $O(1)$ oscillations. This leads to formation of a boundary layer of thickness $O(\epsilon)$ near ∂K [4]. This boundary layer is completely numerical. It is due to the fact that we try to approximate the oscillatory solution of a global elliptic problem by linear superposition of a collection of local base functions whose boundary conditions are not conformed with the oscillatory solution across the edge of the local element.

Note that ϕ_0 corresponds to the base function of the homogenized equation, which does not contain any multiscale feature. Thus, we can approximate ϕ_0 by a simple linear finite element base. If we impose a linear boundary condition for $\phi^\epsilon(\mathbf{x})$ over ∂K, i.e., $\phi^\epsilon|_{\partial K} = \phi_0|_{\partial K}$, then this will induce an oscillatory boundary condition for θ^ϵ:

$$\theta^\epsilon|_{\partial K} = -\phi_1(\mathbf{x},\mathbf{x}/\epsilon)|_{\partial K} \ .$$

As we mentioned earlier, this will introduce a numerical boundary layer to θ^ϵ, which will lead to the so-called resonance error (see discussion below) [27, 20]. To avoid this resonance error, we need to incorporate the multi-dimensional oscillatory information through the cell problem into our boundary condition for ϕ^ϵ, i.e. to set $\phi^\epsilon|_{\partial K} = (\phi_0 + \epsilon\phi_1(\mathbf{x},\mathbf{x}/\epsilon))|_{\partial K}$. In this case, the boundary condition for $\theta^\epsilon|_{\partial K} = 0$. Therefore, we have $\theta^\epsilon \equiv 0$. In this case, we have an analytic expression for the multiscale base functions ϕ^ϵ as follows:

$$\phi^\epsilon = \phi_0(\mathbf{x}) + \epsilon\phi_1(\mathbf{x},\mathbf{x}/\epsilon) \ , \tag{6}$$

with $\phi_1(\mathbf{x},\mathbf{y}) = -\chi^j(\mathbf{x},\mathbf{y}) \frac{\partial \phi_0}{\partial x_j}$ and χ^j is the solution of the cell problem (5).

The above example is to illustrate the difficulty in designing the appropriate boundary condition for the base function. Of course, except for problems with periodic structure, we can not use this approach to compute the multiscale base functions in general. Later we introduce a more effective over-sampling technique to overcome the difficulty of designing the appropriate microscopic boundary conditions for the base functions.

2.3 Convergence Analysis

Convergence analysis has been carried out for the multiscale finite element method in the case when the coefficient, $a^\epsilon(\mathbf{x})$, has a scale separation and periodic structure, although this assumption is not required by our method. What distinguishes our multiscale finite element method from the traditional finite element method is that MsFEM gives a convergence result uniform in ϵ as ϵ tends to zero. To obtain a sharp convergence rate, we need to use the multiscale solution structure given by the homogenization theory [4]. In particular, we rely on a sharp homogenization estimate which uses the boundary corrector [41]. In the case when the boundary conditions of the base functions are linear, we have proved the following convergence result in [28].

Theorem 2.1. *Let $a^\epsilon(\mathbf{x}) = a(\mathbf{x}/\epsilon)$ with $a(\mathbf{y})$ being periodic in $\mathbf{y}$ and smooth. Let $u \in H^2(\Omega)$ be the solution of (1) and u_h be the multiscale finite element approximation obtained from the space spanned by the multiscale bases with linear boundary conditions. Then we have*

$$\|u - u_h\|_{H^1} \leq C(h+\epsilon)\|f\|_{L^2} + C\Big(\frac{\epsilon}{h}\Big)^{1/2}\|u_0\|_{H^2}, \tag{7}$$

where $u_0 \in H^2(\Omega) \cap W^{1,\infty}(\Omega)$ is the solution of the homogenized equation.

We refer to [28] for the detail of the analysis. We remark that convergence analysis for elliptic problems with multiple scales and for problems with random coefficients has been obtained by Efendiev in his Ph.D. dissertation [18]. Moreover, he proved that the above convergence theorem is still valid when the coefficient $(a(\mathbf{y})$ is only piecewise smooth. We would like to point out that in the one-dimensional case the multiscale finite element method can reproduce the exact solution at the coarse grid nodal points without making any assumption of the scale separation and periodic structure of the coefficient [28].

2.4 The over-sampling technique

As we can see from the above theorem, MsFEM indeed gives the correct homogenized result as ϵ tends to zero. This is in contrast with the traditional finite element which does not give the correct homogenized result as $\epsilon \to 0$. For the linear finite element method, the error would grow like $O(h^2/\epsilon^2)$. On the other hand, we also observe that when $h \sim \epsilon$, the multiscale method attains large error in both H^1 and L^2 norms. This is what we call the *resonance* effect between the grid scale,h, and the small scale, ϵ, of the problem. As we indicated earlier, the boundary layer in the first order corrector seems to be the main source of the resonance effect. By a judicious choice of boundary conditions for the base functions, we can eliminate the boundary layer in the first order corrector. This would give a nice conservative difference structure in the discretization, which in turn leads to *cancellation of resonance errors* and gives an improved rate of convergence.

Motivated by our convergence analysis, we propose an *over-sampling* technique to overcome the difficulty due to scale resonance [27]. The idea is quite simple and

easy to implement. The main observation is that the boundary layer in the boundary correction θ^ϵ is *strongly localized*, with the width of order $O(\varepsilon)$. If we sample in a domain with size larger than $h+\varepsilon$ and use only the interior sampled information to construct the bases, we can reduce the influence of the boundary layer in the larger sample domain on the base functions significantly. As a consequence, we obtain an improved rate of convergence.

Specifically, let ψ^j be the base functions satisfying the homogeneous elliptic equation in the larger domain $S \supset K$. We then form the actual base ϕ^i by linear combination of ψ^j,

$$\phi^i = \sum_{j=1}^{d} c_{ij}\psi^j \ .$$

The coefficients c_{ij} are determined by condition $\phi^i(\mathbf{x}_j) = \delta_{ij}$. The corresponding θ^ε for ϕ^i are now free of boundary layers. Our extensive numerical experiments have demonstrated that the over-sampling technique does improve the numerical error substantially in many applications.

Note that the over-sampling technique results in a *non-conforming* MsFEM method. In [20], we perform a careful estimate of the nonconforming errors in both H^1 norm and the L^2 norm. The analysis shows that the non-conforming error is indeed small, consistent with our numerical results [27, 29]. Our analysis also reveals a cell resonance, which is the mismatch between the mesh size and the "perfect" sample size. In case of a periodic structure, the "perfect" sample size is the length of an integer multiple of the period. This cell resonance was first revealed by Santosa and Vogelius in [40]. When the sample size is an integer multiple of the period, then the cell resonance error is identically zero [40, 20]. In the error expansion, this resonance effect appears as a *higher* order correction. In numerical computations, we found that the cell resonance error is generically small, and is almost negligible for random coefficients. Nonetheless, it is possible to completely eliminate this cell resonance error by using a Petrov-Galerkin formulation [52], i.e. to use the over-sampling technique to construct the base functions but using piecewise linear functions as test functions. This reduces the nonconforming error and eliminates the resonance error completely.

We remark that the over-sampling technique is different from the overlapping domain decomposition method. The domain decomposition method is an iterative method to solve the fine grid solution globally, while MsFEM with over-sampling is a method to derive an accurate coarse grid approximation by capturing the effect of small scales on large scales locally. On the other hand, in collaboration with Aarnes [1], we have shown that the multiscale finite element method can be used to construct nearly optimal preconditioner for domain decomposition methods applied to elliptic problems with highly oscillating and high aspect ratio coefficients. Multiscale finite element method has also been used to upscale absolute permeability [51] where we analyze the source of upscaling error in some existing upscaling methods and demonstrate how the over-sampling technique can be used effectively to reduce the upscaling error.

2.5 Convergence and Accuracy

Except for special cases when the coefficient has periodic structure or is separable in space variables, we in general need to compute the multiscale bases numerically using a subgrid mesh. To assess the accuracy of our multiscale method, we compare MsFEM with a traditional linear finite element method (FEM for short) using a subgrid mesh, $h_s = h/M$. The multiscale bases are computed using the same subgrid mesh. Note that MsFEM only captures the solution at the coarse grid h, while FEM tries to resolve the solution at the fine grid h_s. Our extensive numerical experiments demonstrate that the accuracy of MsFEM on the coarse grid h is comparable to that of the corresponding well-resolved FEM calculation at the same coarse grid. In some cases, MsFEM is even more accurate than FEM (see below and the next section).

First, we demonstrate the convergence in the case when the coefficient has scale separation and periodic structure. In Table 1 we present the result for

$$a(\mathbf{x}/\varepsilon) = \frac{2 + P\sin(2\pi x_1/\varepsilon)}{2 + P\cos(2\pi x_2/\varepsilon)} + \frac{2 + \sin(2\pi x_2/\varepsilon)}{2 + P\sin(2\pi x_1/\varepsilon)} \quad (P = 1.8), \tag{8}$$

$$f(\mathbf{x}) = -1 \qquad \text{and} \qquad u|_{\partial\Omega} = 0. \tag{9}$$

The convergence of three different methods are compared for fixed $\varepsilon/h = 0.64$, where "-L" indicates that linear boundary condition is imposed on the multiscale base functions, "os" indicates the use of over-sampling, and LFEM stands for linear FEM.

N	ε	MsFEM-L		MsFEM-os-L		LFEM	
		$\|\|E\|\|_{l^2}$	rate	$\|\|E\|\|_{l^2}$	rate	MN	$\|\|E\|\|_{l^2}$
16	0.04	3.54e-4		7.78e-5		256	1.34e-4
32	0.02	3.90e-4	-0.14	3.83e-5	1.02	512	1.34e-4
64	0.01	4.04e-4	-0.05	1.97e-5	0.96	1024	1.34e-4
128	0.005	4.10e-4	-0.02	1.03e-5	0.94	2048	1.34e-4

Table 1. *Convergence for periodic case.*

We see clearly the scale resonance in the results of MsFEM-L and the (almost) first order convergence (i.e., no resonance) in MsFEM-os-L. Evident also is the error of MsFEM-os-L being smaller than those of LFEM obtained on the fine grid. In [28, 27], more extensive convergence tests have been presented.

Next, we illustrate the convergence of the multiscale finite element method when the coefficient is random and has no scale separation nor periodic structure. In Figure 1, we show the results for a log-normally distributed a^ε. In this case, the effect of scale resonance shows clearly for MsFEM-L, i.e., the error increases as h approaches ε. Here $\varepsilon \sim 0.004$ roughly equals the correlation length. Even the use of an oscillatory boundary conditions (MsFEM-O), which is obtained by solving a reduced 1-D problem along the edge of the element, does not help much in this case. On the other hand, MsFEM with over-sampling agrees very well with

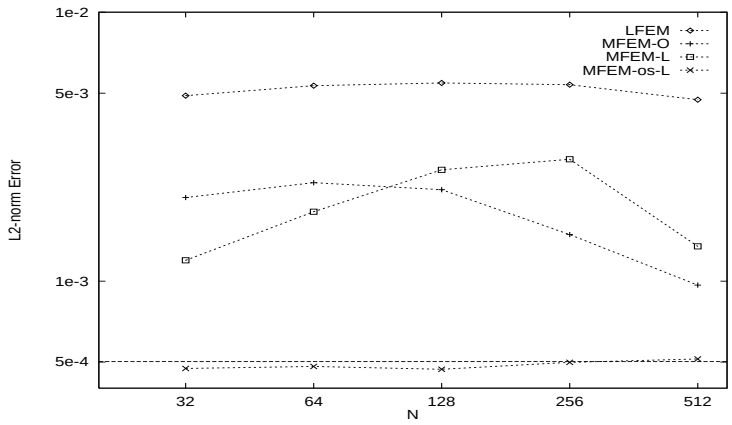

Figure 1. *The l^2-norm error of the solutions using various schemes for a log-normally distributed permeability field.*

the well-resolved calculation. One may wonder why the errors do not decrease as the number of coarse grid elements increases. This is because we use the same subgrid mesh size as the well-resolved grid size to construct the base functions for various coarse grid sizes ($N = 32, 64, 128$, etc). If we use multiscale bases that are obtained analytically or computed with very high precision, then the errors indeed decay as the coarse grid mesh decreases. The above calculations demonstrate that by using locally constructed multiscale finite element bases, we can recover the well-resolved calculation at the coarse grid with comparable accuracy. This is quite remarkable since the local bases are *not* the restrictions of the well-resolved solution of the global elliptic problem to the coarse grid elements. Here the well-resolved calculation corresponds to a 2048 by 2048 linear finite element calculation. The error is computed by extrapolating the 2048×2048 and the 4096×4096 linear finite element solutions. The accuracy of the extrapolated solution is of the order of 10^{-6}.

3 Applications of MsFEM

In this section, we apply the multiscale finite element method to a few applications. The applications we consider are wave propagation in heterogeneous media, convection enhanced diffusion, and flow and transport in heterogeneous porous media.

3.1 Wave Propagation in Heterogeneous Media

The multiscale finite element method can be easily extended to time dependent wave equation. Wave propagation in heterogeneous media is an important problem that has rich multiscale phenomena and a wide range of applications in geoscience and medical imaging.

Consider the wave equation in a heterogeneous media:

$$\frac{\partial^2 u}{\partial t^2} = \nabla \cdot a^\epsilon(\mathbf{x}) \nabla u + F(\mathbf{x}, t) \ , \quad u|_{t=0} = f(\mathbf{x}), \quad (u_t)|_{t=0} = g(\mathbf{x}) \ .$$

For this wave equation, we can construct the multiscale finite element bases in the same way as we did for the elliptic problem, i.e.

$$\nabla \cdot a^\epsilon(\mathbf{x}) \nabla \phi^\epsilon = 0 \, ,$$

with appropriate boundary condition on the edge of each element K (e.g. using the over-sampling technique).

Using a similar coefficient as in Table 1 and with zero forcing, we have performed the following convergence study (the work described in this subsection was carried out by a former postodc, Dr. Yu Zhang). In this study, we choose $\epsilon = 0.005$, and the well-resolved calculation is obtained by using a 2048×2048 fine grid. We compare the multiscale finite element calculation with both the well-resolved solution, denoted as u, and the homogenized solution, denoted as u_0. We can see that the multiscale finite element calculations converge to the well-resolved solution with a rate comparable to that for the homogenized solution.

N	$\|u_h - u\|$	$\|u_h - u_0\|$
32	0.03068	0.030370
64	0.01435	0.013994
128	0.0067795	0.00646126
256	0.0031569	0.00281998

Table 2. *Errors of multiscale finite element calculations for the wave equation with periodic oscillating coefficient.*

We have also computed the wave equation with a random coefficient which has a continuous spectrum of scale and has a fractal dimension of 2.8 (see [27] for a description of this random medium). The initial condition is given as a symmetric Gaussian pulse with zero initial velocity. For deterministic homogeneous media, it is known that the solution will remain symmetric in time. But for random homogeneous media, we found that the solution develops asymmetry in its wave front dynamically, which is completely due to the randomness of the wave speed coefficient.

The computational cost for the wave propagation using MsFEM is significantly reduced compared with the direct simulation using a fine grid. This is because the computational cost in computing the multiscale bases is only at time $t = 0$. Once we have generated the multiscale bases initially, we can compute the corresponding stiffness matrix for the coarse grid. The subsequent calculations are all done using a coarse spatial grid and a coarse time step. In comparison, a fine grid with small time step must be used for each fine grid simulation. The saving can be quite significant.

3.2 Convection Enhanced Diffusion

Another interesting application is the large time behavior of the convection diffusion equation with a rapidly oscillating velocity field and a slowly varying initial

condition:

$$\frac{\partial T}{\partial t} + \mathbf{u}_\delta(\mathbf{x}) \cdot \nabla T = \epsilon \triangle T \ , \quad T(\mathbf{x}, 0) = T_0(\delta \mathbf{x}),$$

where the velocity field $\mathbf{u}_\delta$ is divergence-free and δ characterizes the small scale in the velocity field. After rescaling the space and time variables, $\mathbf{x}' = \mathbf{x}/\delta$ and $t' = t/\delta^2$, we obtain the rescaled convection diffusion as follows (still use $\mathbf{x}$ and t):

$$\frac{\partial T}{\partial t} + \mathbf{u}(\mathbf{x}/\delta) \cdot \nabla T = \epsilon \triangle T \ , \quad T(\mathbf{x}, 0) = T_0(\mathbf{x}).$$

Under appropriate assumption on $\mathbf{u}$ (see, e.g. [23]), it can be shown that T^δ converges to an effective solution T^* as δ tends to zero for each $\epsilon > 0$ fixed:

$$\frac{\partial T^*}{\partial t} = \sigma_\epsilon \triangle T^* \ , \quad T^*(\mathbf{x}, 0) = T_0(\mathbf{x}).$$

We call σ_ϵ the effective diffusivity. In general, we have $\sigma_\epsilon > \epsilon$. How does σ_ϵ scale with ϵ as ϵ tends to zero is a problem of considerable interest. The answer depends on the geometry of the streamlines associated with the velocity field $\mathbf{u}$.

One of the well-known cases is the cellular flow in which the stream function is given by

$$H(\mathbf{x}) = \frac{1}{4\pi^2} \sin(2\pi x_1/\delta) \sin(2\pi x_2/\delta) \ ,$$

and the velocity field is given by $\mathbf{u} = (-H_{x_2}, H_{x_1})$. In this case, it has been shown analytically that $\sigma_\epsilon \sim C\sqrt{\epsilon}$ as $\epsilon \to 0$ (see e.g. [22]).

In the Ph.D. dissertation of Dr. Peter Park [42], he has applied the multiscale finite element method to compute the effective diffusivity as $\epsilon \to 0$. The multiscale bases are constructed by satisfying the following steady equation:

$$\mathbf{u}(\mathbf{x}/\delta) \cdot \nabla \phi^\epsilon = \epsilon \triangle \phi^\epsilon \ ,$$

with appropriate boundary conditions. By applying the Galerkin finite element method with the above multiscale bases and discretizing in time implicitly, we can obtain a finite element discretization similar to that considered before.

To compute the effective diffusivity, we use the following formula [22]

$$\sigma_\epsilon = \lim_{t \to \infty} \frac{1}{4t} \int \int (|\mathbf{x}|^2 T(\mathbf{x}, t)) \, d\mathbf{x} \ ,$$

with initial condition equal to a Dirac delta function $T_0 = \delta(\mathbf{x})$. With a relatively coarse grid (16 by 16) and a subgrid $h_s = 1/512$, we obtain the following results for the effective diffusivity σ_ϵ for different values of δ and ϵ in Table 3 [42].

As we can see from Table 3, when the velocity field is smooth, i.e. $\delta = 1$, the effective diffusivity is of the same order as the molecular diffusivity ϵ, i.e. $\sigma_\epsilon \sim C\epsilon$. But for highly oscillating velocity field with small δ ($\delta = 0.01$), we see that the effective diffusivity reveals the scaling $\sigma_\epsilon \sim C\sqrt{\epsilon}$ as ϵ tends to zero (note that $\frac{1}{\sqrt{2}} \sim 0.7071$). This verifies the theoretical result for the effective diffusivity for the cellular flow. Since the velocity field is steady, the multiscale bases are computed

ϵ	σ_ϵ	ratio	σ_ϵ	ratio	σ_ϵ	ratio
	$\delta = 1$		$\delta = 0.1$		$\delta = 0.05$	
0.04	0.03252		0.03265		0.03275	
0.02	0.02092	0.6432	0.02316	0.7093	0.02355	0.7191
0.01	0.01141	0.5454	0.01643	0.7094	0.01665	0.7070
0.005	0.00619	0.5425	0.01300	0.7912	0.01233	0.7405
0.0025	0.00344	0.5557	0.01046	0.8046	0.00872	0.7072

Table 3. *The diffusivity scaling for the cellular flow.*

only at $t = 0$. The subsequent computation in time uses a coarse grid in space ($H = 1/16$) and a large time step. This is much cheaper than performing the calculation using a fine space grid which has to resolve δ and uses a small time step.

In this particular example, we can solve the corresponding cell problem to construct the multiscale bases, which leads to additional computational saving. In general, the velocity field is generated by solving the Navier-Stokes equation, whose solution would not have scale separation nor periodic structure. For certain random velocity, the convection diffusion equation may exhibit anomalous diffusion behavior (see, e.g. [23]). The effective diffusivity may depend on some nonlocal geometric property of the velocity field. We have also investigated the anomalous diffusion induced by a nonlocal random velocity field by supplementing the local multiscale bases with a nonlocal base to capture the nonlocal interaction of small scales [42].

3.3 Flow and Transport in Porous Media

The flow and transport problems in porous media are considered in a hierarchical level of approximation. At the microscale, the solute transport is governed by the convection-diffusion equation in a homogeneous fluid. However, for porous media, it is very difficult to obtain full information about the pore structure. Certain averaging procedure has to be carried out, and the porous medium becomes a continuum with certain macroscopic properties, such as the porosity and permeability. Through the use of sophisticated geological and geostatistical modeling tools, engineers and geologists can now generate highly detailed, three dimensional representations of reservoir properties. Such models can be particularly important for reservoir management, as fine scale details in formation properties, such as thin, high permeability layers or thin shale barriers, can dominate reservoir behavior. The direct use of these highly resolved models for reservoir simulation is not generally feasible because their fine level of detail (tens of millions grid blocks) places prohibitive demands on computational resources. Therefore, the ability to coarsen these highly resolved geologic models to levels of detail appropriate for reservoir simulation (tens of thousands grid blocks), while maintaining the integrity of the model for purpose of flow simulation (i.e., avoiding the loss of important details), is clearly needed.

We consider a heterogeneous system which represents two-phase immiscible

flow. Our interest is in the effect of permeability heterogeneity on two-phase flow. Therefore, we neglect the effect of compressibility and capillary pressure, and consider porosity to be constant. This system can be described by writing Darcy's law for each phase (all quantities are dimensionless):

$$\mathbf{v}_j = \frac{k_{rj}(S)}{\mu_j}\mathcal{K}^\epsilon \nabla p, \tag{10}$$

where $\mathbf{v}_j$ are the Darcy's velocity for the phase j ($j = o, w$ oil, water), p is pressure, S is water saturation, K^ϵ is the permeability tensor, k_{rj} is the relative permeabilities of each phase and μ_j is the viscosity of the phase j. The Darcy's law for each phase coupled with mass conservation, can be manipulated to give the pressure and saturation equations:

$$\nabla \cdot (\lambda(S)\mathcal{K}^\epsilon \nabla p) = 0, \tag{11}$$

$$\frac{\partial S}{dt} + \mathbf{u}^\epsilon \cdot \nabla f(S) = 0, \tag{12}$$

which can be solved subject to some appropriate initial and boundary conditions. The parameters in the above equations are given by

$$\lambda = \frac{k_{rw}(S)}{\mu_w} + \frac{k_{ro}(S)}{\mu_o}, \tag{13}$$

$$f(S) = \frac{k_{rw}(S)/\mu_w}{k_{rw}(S)/\mu_w + k_{ro}/\mu_o}, \tag{14}$$

$$\mathbf{u}^\epsilon = \mathbf{v}_w + \mathbf{v}_o = -\lambda(S)K^\epsilon \nabla p. \tag{15}$$

Fine Scale Recovery

To solve transport problems in the subsurface formations, as in oil reservoir simulations, one needs to compute the velocity field from the elliptic equation for pressure, i.e $\mathbf{u}^\epsilon = -\lambda(S)\mathcal{K}^\epsilon \nabla p$. In some applications involving isotropic media, the cell-averaged velocity is sufficient, as shown by some computations using the local upscaling methods (cf. [15]). However, for anisotropic media, especially layered ones (Figure 2), the velocity in some thin channels can be much higher than the cell average, and these channels often have dominant effects on the transport solutions. In this case, the information about fine scale velocity becomes vitally important. Therefore, an important question for all upscaling methods is how to take those fast-flow channels into account.

For MsFEM, the fine scale velocity can be easily recovered from the multiscale base functions, noting that they provide interpolations from the coarse h-grid to the fine h_s-grid. To demonstrate the accuracy of the recovered velocity and effect of small-scale velocity on the transport problem, we show the fractional flow result of a "tracer" test using the layered medium in Figure 2: a fluid with red color originally saturating the medium is displaced by the same fluid with blue color injected by flow in the medium at the left boundary, where the flow is created by a unit horizontal

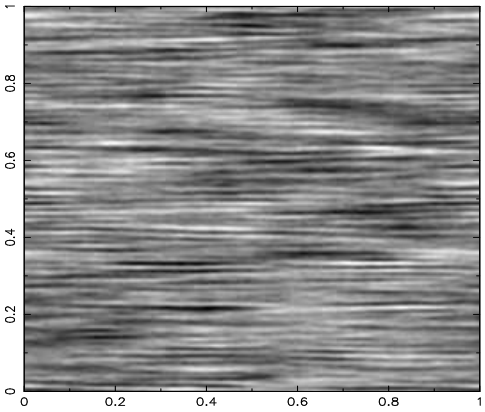

Figure 2. *A random porosity field with layered structure.*

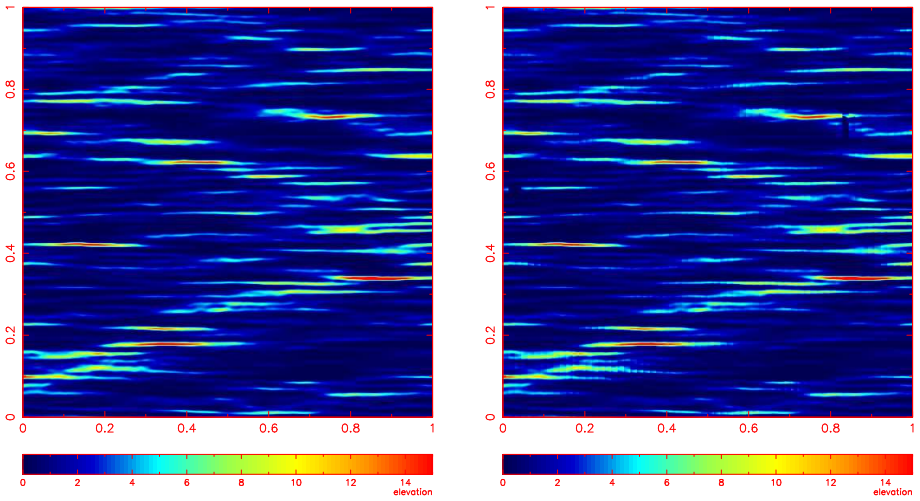

Figure 3. *(a): Fine grid horizontal velocity field, $N = 1024$. (b): Recovered horizontal velocity field from the coarse grid calculation ($N = 64$) using multiscale bases.*

pressure drop. The transport equation is solved to compute the saturation of the red fluid (see [16] for more details).

To illustrate that we can recover the fine grid velocity field from the coarse grid pressure calculation, we plot the horizontal velocity fields obtained by two methods. In Figure 3a, we plot the horizontal velocity field obtained by using a fine grid ($N = 1024$) calculation. In Figure 3b, we plot the same horizontal velocity field obtained by using the coarse grid pressure calculation with $N = 64$ and using the multiscale finite element bases to interpolate the fine grid velocity field. We can see that the recovered velocity field captures very well the layer structure in the fine grid

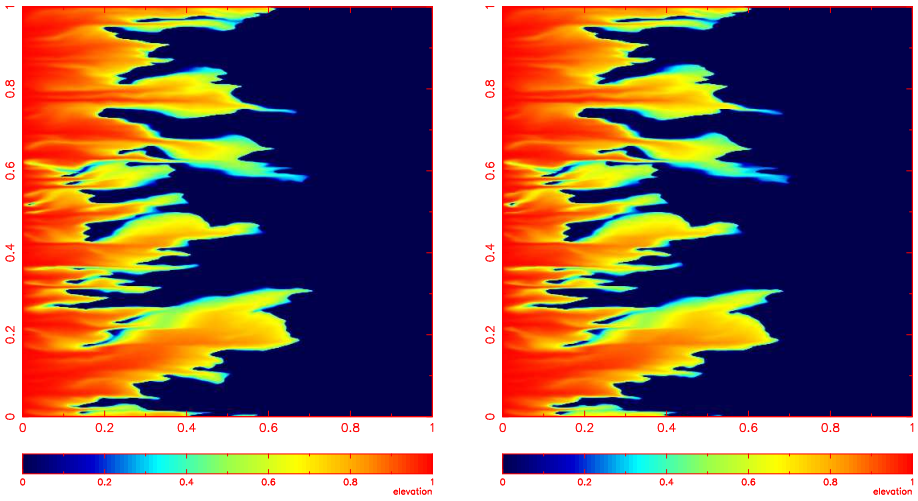

Figure 4. *(a): Fine grid saturation at* $t = 0.06$, $N = 1024$. *(b): Saturation computed using the recovered velocity field from the coarse grid calculation* ($N = 64$) *using multiscale bases.*

velocity field. Further, we use the recovered fine grid velocity field to compute the saturation in time. In Figure 4a, we plot the saturation at $t = 0.06$ obtained by the fine grid calculation with $N = 1024$. Figure 4b shows the corresponding saturation obtained using the recovered velocity field from the coarse grid calculation with $N = 64$. Most detail fine scale fingering structures in the well-resolved saturation are captured very well by the corresponding calculation using the recovered velocity field from the coarse grid pressure calculation. The agreement is striking.

We also check the fractional flow curves obtained by the two calculations. The fractional flow of the red fluid, defined as $F = \int S_{red} u_1^\epsilon \, dy / \int u_1^\epsilon \, dy$ (S being the saturation, u_1^ϵ being the horizontal velocity component), at the right boundary is shown in Figure 5. The top pair of curves are the solutions of the transport problem using the cell-averaged velocity obtained from a well-resolved solution and from MsFEM; the bottom pair are solutions using well-resolved fine scale velocity and the recovered fine scale velocity from the MsFEM calculation. Two conclusions can be made from the comparisons. First, the cell-averaged velocity may lead to a large error in the solution of the transport equation. Second, both the recovered fine scale velocity and the cell-averaged velocity obtained from MsFEM give faithful reproductions of respective direct numerical solutions.

We remark that a finite volume version of the multiscale finite element method has been developed by the petroleum engineers from Chevron Petroleum Technology Co. [34]. They also found that by updating the multiscale bases adaptively in space and time, they can recover the fine scale detail of the well-resolved calculation. The percentage of the multiscale bases that need to be updated is small (only a few percent of the total number of bases). In some sense, the multiscale finite element method also offers an efficient approach to capture the fine scale details using only a

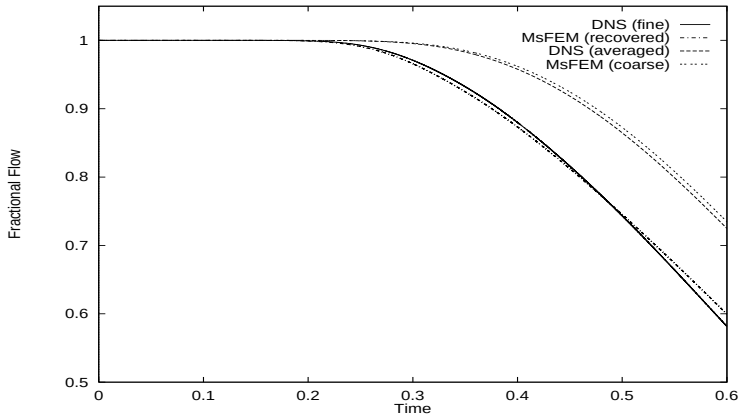

Figure 5. *Variation of fractional flow with time. DNS: well-resolved direct numerical solution using LFEM ($N = 512$). MsFEM: over-sampling is used ($N = 64$, $M = 8$).*

small fraction of the computational time required for a direct numerical simulation using a fine grid.

3.4 Scale-up of one-phase flows

The multiscale finite element method has been used in conjunction with some moment closure models to obtain an upscaled method for one-phase flows, see, e.g. [18, 19, 9]. Note that the multiscale finite element method presented above does not conserve mass exactly. For long time integration, it may lead to loss of mass. This is an undesirable feature of the method. In a recent work with Dr. Zhiming Chen [9], we have designed and analyzed a mixed multiscale finite element method. We then applied this mixed method to study the scale up of one-phase flows and found that mass is conserved very well even for long time integration. Below we describe our results in some detail.

In its simplest form, neglecting the effect of gravity, compressibility, capillary pressure, and considering constant porosity and unit mobility, the governing equations for the flow transport in highly heterogeneous porous media can be described by the following partial differential equations ([35],[47],[18])

$$\nabla \cdot (\mathcal{K}^\epsilon(\mathbf{x})\nabla p) = 0, \tag{16}$$

$$\frac{\partial S}{\partial t} + \mathbf{u}^\epsilon \cdot \nabla S = 0, \tag{17}$$

where p is the pressure, S is the water saturation, $\mathcal{K}^\epsilon(\mathbf{x}) = (\mathcal{K}^\epsilon_{ij}(\mathbf{x}))$ is the relative permeability tensor, and $\mathbf{u}^\epsilon = -\mathcal{K}(\mathbf{x})\nabla p$ is the Darcy velocity.

Now we describe how the (mixed) multiscale finite element can be combined with the existing upscaling technique for the saturation equation (17) to get a complete coarse grid algorithm for the problem (16)-(17). The numerical upscaling of the saturation equation has been under intensive study in the literature

[16, 19, 35, 26, 48, 49]. The problem is very challenging mathematically without capillary pressure because of the nonlocal memory effect [46]. On the other hand, if the capillary effect becomes important, the saturation equation becomes diffusion dominated transport. In this case, homogenization result has been obtained [5] and numerical upscaling method can be designed [2].

In many oil reservoir applications, capillary effect is so small that it is neglected in practice. So we must face the nonlocal memory effect induced by the convection dominated transport. Here we use the upscaling method proposed in [19] and [18] to design an overall coarse grid model for the problem (16)-(17). The work of [19] for upscaling the saturation equation involves a moment closure argument. The velocity and the saturation are separated into a local mean quantity and a small scale perturbation with zero mean. For example, the Darcy velocity is expressed as $\mathbf{u}^\epsilon = \mathbf{u}_0 + \mathbf{u}'$ in (17), where $\mathbf{u}_0$ is the average of velocity $\mathbf{u}$ over each coarse element, $\mathbf{u}'$ is the deviation of the fine scale velocity from its coarse scale average. If one ignores the third order terms containing the fluctuations of velocity and saturation, one can obtain an average equation for the saturation S as follows [19]:

$$\frac{\partial S}{\partial t} + \mathbf{u}_0 \cdot \nabla S = \frac{\partial}{\partial x_i}\Big(D_{ij}(\mathbf{x},t)\frac{\partial S}{\partial x_j}\Big), \tag{18}$$

where the diffusion coefficients $D_{ij}(\mathbf{x},t)$ are defined by

$$D_{ii}(\mathbf{x},t) = \langle|\mathbf{u}_i'(\mathbf{x})|\rangle L_i^0(\mathbf{x},t), \quad D_{ij}(\mathbf{x},t) = 0, \quad \text{for } i \neq j,$$

where $\langle|\mathbf{u}_i'(\mathbf{x})|\rangle$ stands for the average of $|\mathbf{u}_i'(\mathbf{x})|$ over each coarse element. The function $L_i^0(\mathbf{x},t)$ is the length of the coarse grid streamline in the x_i direction which starts at time t at point $\mathbf{x}$, i.e.

$$L_i^0(\mathbf{x},t) = \int_0^t y_i(s)\,ds,$$

where $\mathbf{y}(s)$ is the solution of the following system of ODEs

$$\frac{d\mathbf{y}(s)}{ds} = \mathbf{u}_0(\mathbf{y}(s)), \quad \mathbf{y}(t) = \mathbf{x}.$$

Note that the hyperbolic equation (17) is now replaced by a convection-diffusion equation. One should note that the induced diffusion term is history dependent. In some sense, it captures the nonlocal history dependent memory effect described by Tartar in the simple shear flow problem [46]. The convection diffusion equation (18) will be solved by the characteristic linear finite element method [14, 43] in our simulation.

The mixed multiscale finite element method can be readily combined with the above upscaling model for the saturation equation. The local fine grid velocity $\mathbf{u}'$ can be reconstructed from the multiscale finite element bases. We perform a coarse grid computation of the above algorithm on the coarse 64×64 mesh. The fractional flow curve using the above algorithm is depicted in Figure 6. It gives excellent agreement with the "exact" fractional flow curve which is obtained using a fine

1024×1024 mesh. We also compare the contour plots of the saturation S obtained by the upscaled equation with those obtained by using a well-resolved calculation. We found that the the upscaled saturation captures the overall large scale structure of the fine grid saturation, but the sharp oil/water interfaces are smeared out. This is due to the parabolic nature of the upscaled equation (18).

The main cost in the above algorithm lies in the computation of multiscale bases which can be done *a priori* and completely in parallel. This algorithm is particularly attractive when multiple simulations must be carried out due to the change of boundary and source distribution as it is often the case in engineering applications. In such a situation, the cost of computing the multiscale base functions is just an over-head. Moreover, once these base functions are computed, they can be used for subsequent time integration of the saturation. Because the evolution equation is now solved on a coarse grid, a larger time step can be used. This also offers additional computational saving. For many oil recovery problems, due to the excessively large fine grid data, upscaling is a necessary step before performing many simulations and realizations on the upscaled coarse grid model. If one can coarsen the fine grid by a factor of 10 in each dimension, the computational saving of the coarse grid model over the original fine model could be as large as a factor 10,000 (three space dimensions plus time).

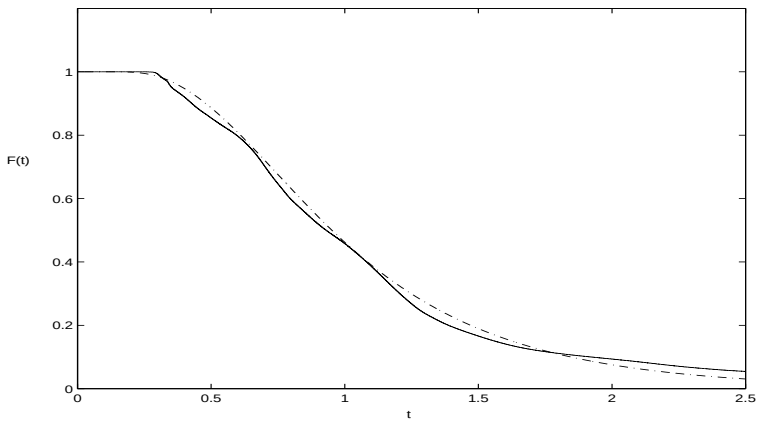

Figure 6. *The accuracy of the coarse grid algorithm. Solid line is the well-resolved fractional flow curve. The slash-dotted line is the fractional flow curve using above coarse grid algorithm.*

Upscaling the two-phase flow

Upscaling the two-phase flow is more difficult due to the dynamic coupling between the pressure and the saturation. One important observation is that the fluctuation in saturation is relatively small away from the oil/water interface. In this region, the multiscale bases are essentially the same as those generated by the corresponding one-phase flow (time independent). In practice, we can design an adaptive strategy to update the multiscale bases in space and time. The percentage of multiscale bases that need to be updated is relatively small (a few percent of

the total number of the bases). The upscaling of the saturation equation based on moment closure argument can be generalized to the two-phase flow as long as the fluctuation of the velocity field $\mathbf{u}'$ can be accurately recovered from the coarse grid computation [35, 19]. As we discussed from the previous subsection, this is indeed one of the main advantages of the multiscale finite element method.

It remains to develop a more systematic multiscale analysis to upscale the two-phase flow with heterogeneous media. While the upscaled saturation equation based on moment closure approximation is simple and easy to implement, it is hard to estimate its modeling error as the fluctuations in velocity or saturation are not small in practice. With Dr. Danping Yang [31], we have recently developed a new multiscale analysis for convection dominated transport equation which allows us to upscale the saturation without making the moment closure approximation. It is based on a delicate multiscale analysis of the transport equation. We are now trying to generalize the analysis to the two-phase flow [50]. The objective is to derive a systematic upscaling for the two-phase flow in heterogeneous porous media which do not have scale separation or periodic structure.

4 Nonlinear homogenization for 3-D Euler equations

The upscaling of the nonlinear transport equation in two-phase flows shares some of the common difficulties in deriving the effective equations for the incompressible Euler equations. With Dr. Danping Yang [30], we have recently developed a systematic multiscale analysis for the incompressible 3-D Euler equations. The understanding of scale interactions for 3-D incompressible Euler and Navier-Stokes equations has been a major challenge. For high Reynolds number flows, the degrees of freedom are so high that it is almost impossible to resolve all small scales by direct numerical simulations. Deriving an effective equation for the large scale solution is very useful in engineering applications, see e.g. [45, 36, 12, 25]. In deriving a large eddy simulation model, one usually needs to make certain closure assumptions. The accuracy of such closure models is hard to measure *a priori*. It varies from application to application. For many engineering applications, it is desirable to design a subgrid-based large scale model in a systematic way so that we can measure and control the modeling error. The main difficulty in deriving effective equations systematically is the strong nonlinear interaction of small scales and the lack of scale separation. Our ultimate goal is to develop a new multiscale analysis that can effectively average infinitely many scales without assuming scale separation. The challenge is to do this in such a way that we can account for the modeling error systematically when averaging out small scales.

We consider the 3-D incompressible Navier-Stokes equation

$$\mathbf{u}^\epsilon_t + (\mathbf{u}^\epsilon \cdot \nabla)\mathbf{u}^\epsilon + \nabla p^\epsilon = \nu \triangle \mathbf{u}^\epsilon, \tag{19}$$

$$\nabla \cdot \mathbf{u}^\epsilon = 0, \tag{20}$$

with multiscale initial data $\mathbf{u}^\epsilon(\mathbf{x}, 0) = \mathbf{u}^\epsilon_0(\mathbf{x})$. Here $\mathbf{u}^\epsilon(t, \mathbf{x})$ and $p^\epsilon(t, \mathbf{x})$ are velocity and pressure respectively, ν is viscosity. For the time being, we consider only the infinite domain and assume that the solution decays to zero sufficiently fast at

infinity. As a first step, we assume that the initial condition has scale separation and periodic structure. That is, we assume that $\mathbf{u}^\epsilon(\mathbf{x},0) = \mathbf{U}(\mathbf{x}) + \mathbf{W}(\mathbf{x}, \frac{\mathbf{x}}{\epsilon})$. Moreover we assume that $\mathbf{U}$ and $\mathbf{W}$ are smooth, $\mathbf{W}(\mathbf{x},\mathbf{y})$ is periodic in $\mathbf{y}$ and has mean zero. In order for the small scale solution to survive the diffusion, the viscosity ν must be of the order $O(\epsilon^2)$. In this case, the diffusion term will not enter the homogenized equation nor the cell problem. To simplify the derivation, we consider only the inviscid case with $\nu = 0$. The question of interest is how to derive a homogenized equation for the averaged velocity field as $\epsilon \to 0$.

The homogenization of the Euler equation with oscillating data was first studied by McLaughlin-Papanicolaou-Pironneau (MPP for short) in 1985 [39]. Since the Euler equation is nonlinear and nonlocal, it is not clear whether the solution will preserve the two-scale structure of the initial data dynamically. Intuitively, nonlinear interaction may generate new scales dynamically. Therefore constructing an appropriate multiscale expansion for the nonlinear Euler equation is a difficult task. Motivated by some physical argument, MPP made the assumption that the small scale oscillation is convected by the mean flow. Based on this assumption, they made the following multiscale expansions for velocity and pressure:

$$\mathbf{u}^\epsilon(\mathbf{x},t) = \mathbf{u}(\mathbf{x},t) + \mathbf{w}(\mathbf{x},t,\frac{\theta(\mathbf{x},t)}{\epsilon},\frac{t}{\epsilon}) + \epsilon\mathbf{u}_1(\cdot\cdot,\frac{\theta(\mathbf{x},t)}{\epsilon},\frac{t}{\epsilon}) + \cdots$$
$$p^\epsilon(\mathbf{x},t) = p(\mathbf{x},t) + \pi(\mathbf{x},t,\frac{\theta(\mathbf{x},t)}{\epsilon},\frac{t}{\epsilon}) + \epsilon p_1(\cdot\cdot,\frac{\theta(\mathbf{x},t)}{\epsilon},\frac{t}{\epsilon}) + \cdots$$

where $\mathbf{w}(\mathbf{x},t,\mathbf{y},\tau)$, $\mathbf{u}_1(\mathbf{x},t,\mathbf{y},\tau)$, π, and p_1 are assumed to be periodic in both $\mathbf{y}$ and τ, and the phase θ is convected by the mean velocity field $\mathbf{u}$

$$\frac{\partial\theta}{\partial t} + \mathbf{u}\cdot\nabla_{\mathbf{x}}\theta = 0, \quad \theta(\mathbf{x},0) = \mathbf{x}\ . \tag{21}$$

By substituting the above multiscale expansions into the Euler equation and equating coefficients of the same order, MPP obtained a periodic cell problem for $\mathbf{w}(\mathbf{x},t,\mathbf{y},\tau)$, $\mathbf{u}_1(\mathbf{x},t,\mathbf{y},\tau)$, π, and p_1. On the other hand, it is not clear whether the resulting cell problem for $\mathbf{w}(\mathbf{x},t,\mathbf{y},\tau)$, etc has a solution that is periodic in both $\mathbf{y}$ and τ. Even if such solution exists, it may not be unique. Additional assumptions were imposed on the solution of the cell problem in order to derive a variant of the $k-\epsilon$ model. Instead of using the rate of energy dissipation ϵ, they used the mean helicity together with the mean kinetic energy k to derive a closure for the mean velocity equation.

The idea of introducing a phase function in the multiscale expansion to describe the propagation of small scale velocity field is ingenious and insightful. If one naively looks for multiscale expansion in the form of $\mathbf{w}(t,\mathbf{x},t/\epsilon,\mathbf{x}/\epsilon)$, then one would not be able to derive a well-posed cell problem for the $(\tau,\mathbf{y})$ variables (here $\tau = t/\epsilon, \mathbf{y} = \mathbf{x}/\epsilon$).

With Dr. Danping Yang [30], we have recently revisited this problem. Our study shows that the phase variable θ^ϵ should be convected by the full oscillatory velocity field, $\mathbf{u}^\epsilon$:

$$\frac{\partial\theta^\epsilon}{\partial t} + \mathbf{u}^\epsilon\cdot\nabla_{\mathbf{x}}\theta^\epsilon = 0, \quad \theta^\epsilon(\mathbf{x},0) = \mathbf{x}\ . \tag{22}$$

This becomes obvious when we formulate the 2-D Euler equations in vorticity form

$$\omega(\mathbf{x},t) = \tilde{\omega}_0(\theta^\epsilon(\mathbf{x},t), \frac{\theta^\epsilon(\mathbf{x},t)}{\epsilon}),$$

where $\tilde{\omega}_0$ is the initial vorticity. Similar conclusion can be drawn for the 3-D Euler equation, see below. On the other hand, it is not clear what is the multiscale structure of $\theta^\epsilon(\mathbf{x},t)$ since its structure is coupled to the multiscale structure of $\mathbf{u}^\epsilon$. By allowing θ^ϵ develops multiscale structure, we embed multiscale structure within multiscale expansions. This approach is quite nonconventional. To derive a well-posed cell problem is quite a challenge. If one naively expands $\theta^\epsilon(\mathbf{x},t)$ into

$$\theta^\epsilon(\mathbf{x},t) = \theta_0(\mathbf{x},t) + \epsilon\theta_1(\mathbf{x},t,\frac{\mathbf{x}}{\epsilon},\frac{t}{\epsilon}) + \cdots, \tag{23}$$

it will lead to generation of infinite number of scales at $t > 0$. On the other hand, it is clear that if we substitute a multiscale expansion of θ^ϵ into the velocity field, the first order correction term θ_1 would have $O(1)$ contribution to the oscillatory velocity field, $\mathbf{w}$, which in turn will contribute to the averaged solution $\mathbf{u}$.

Lagrangian description of the Euler equations

The key idea in our multiscale analysis for the Euler equation is to reformulate the problem using θ^ϵ as a new variable. The multiscale structure of the solution becomes very apparent in terms of the θ^ϵ variable. This amounts to using a Lagrangian description of the Euler equations. Specifically, we introduce a change of variables from $\mathbf{x}$ to α: $\alpha = \theta^\epsilon(\mathbf{x},t)$. It is easy to see that the inverse of this map, denoted as $\mathbf{x} = \mathbf{X}^\epsilon(\alpha,t)$, is the Lagrangian flow map:

$$\frac{\partial \mathbf{X}^\epsilon(\alpha,t)}{\partial t} = \mathbf{u}^\epsilon(\mathbf{X}^\epsilon(\alpha,t),t), \quad \mathbf{X}^\epsilon(\alpha,0) = \alpha. \tag{24}$$

In terms of the α variable, the vorticity of the 3-D Euler equation has a simple expression (see, e.g., page 32 of [11]):

$$\omega^\epsilon(\mathbf{X}^\epsilon(\alpha,t),t) = \frac{\partial \mathbf{X}^\epsilon}{\partial \alpha}(\alpha,t)\tilde{\omega}_0(\alpha,\frac{\alpha}{\epsilon}) \ , \tag{25}$$

where $\omega^\epsilon = \nabla_x \times \mathbf{u}^\epsilon$ is vorticity, and $\tilde{\omega}_0$ is the initial vorticity. Velocity can be computed from the stream function ψ^ϵ, i.e. $\mathbf{u}^\epsilon = \nabla_x \times \psi^\epsilon$. Further, the stream function, ψ^ϵ, satisfies

$$-\triangle_{\mathbf{x}}\, \psi^\epsilon = \omega^\epsilon \ .$$

In terms of the α variable, we have

$$-\nabla_\alpha \cdot \mathcal{A}\mathcal{A}^T \nabla_\alpha \psi^\epsilon = \frac{\partial \mathbf{X}^\epsilon}{\partial \alpha}(\alpha,t)\tilde{\omega}_0(\alpha,\frac{\alpha}{\epsilon}) \ , \tag{26}$$

where $\mathcal{A} = \left(\frac{\partial \mathbf{X}^\epsilon}{\partial \alpha}\right)^{-1}$. Using $|\frac{\partial \mathbf{X}^\epsilon}{\partial \alpha}| = 1$, we can express $\mathcal{A}$ in terms of $\frac{\partial \mathbf{X}^\epsilon}{\partial \alpha}$. Now we can see clearly that the small scale solution is propagated along the Lagrangian trajectory as a function of α/ϵ.

4.1 Multiscale analysis in Lagrangian frame

The objective of our multiscale analysis is to obtain an averaged equation for the well-mixing long time solution of the Euler equations. For this reason, we look for multiscale solutions of the form ($\mathbf{y} = \alpha/\epsilon$, $\tau = t/\epsilon$):

$$\psi^\epsilon = \psi^{(0)}(t,\alpha) + \epsilon\psi^{(1)}(t,\alpha,\tau,\mathbf{y}) + O(\epsilon^2)\ ,$$
$$\mathbf{X}^\epsilon = \mathbf{X}^{(0)}(t,\alpha) + \epsilon\mathbf{X}^{(1)}(t,\alpha,\tau,\mathbf{y}) + O(\epsilon^2),$$

where $\psi^{(1)}$ and $\mathbf{X}^{(1)}$ are periodic functions with respect to $\mathbf{y}$ and have zero mean.

By performing careful multiscale analysis, we can obtain the homogenized equations for both 2-D and 3-D Euler equations. For simplicity, we only state the main result for the 2-D Euler equation. In the 3-D Euler equation, there will be interaction between the small scales in the Jacobian of the Lagrangian flow map and the multiscale initial vorticity, which reflects the effect of vortex stretching. Such effect is absent in the 2-D Euler equation. For the 2-D Euler equation, the homogenized equations for $\mathbf{X}^{(0)}$, $\mathbf{X}^{(1)}$, and $\psi^{(0)}$, $\psi^{(1)}$ are given as follows:

$$\partial_t \mathbf{X}^{(0)} - \nabla_\alpha \mathbf{X}^{(0)} \nabla_\alpha^\perp \psi^{(0)} = 0, \quad \mathbf{X}^{(0)}|_{\tau=0} = \alpha, \tag{27}$$
$$\partial_\tau \mathbf{X}^{(1)} - \nabla_{\mathbf{y}} \mathbf{X}^{(1)} (\nabla_\alpha^\perp \psi^{(0)} + \nabla_{\mathbf{y}}^\perp \psi^{(1)}) = \nabla_\alpha \mathbf{X}^{(0)} \nabla_{\mathbf{y}}^\perp \psi^{(1)}, \quad \mathbf{X}^{(1)}|_{\tau=0} = \mathbf{0}, \tag{28}$$

$$\nabla_{\mathbf{y}} \cdot (\mathcal{A}_0 \mathcal{A}_0^T \nabla_{\mathbf{y}} \psi^{(1)}) + \nabla_{\mathbf{y}} \cdot (\mathcal{A}_0 \mathcal{A}_0^T \nabla_\alpha \psi^{(0)}) = \omega_0, \tag{29}$$
$$\nabla_\alpha \cdot (\langle \mathcal{A}_0 \mathcal{A}_0^T \rangle \nabla_\alpha \psi^{(0)}) = \langle \omega_1 \rangle - \nabla_\alpha \cdot (\langle \mathcal{A}_0 \mathcal{A}_0^T \nabla_{\mathbf{y}} \psi^{(1)} \rangle), \tag{30}$$

where $\nabla_\alpha^\perp = (-\partial_{\alpha_2}, \partial_{\alpha_1})$, $\omega_0 = curl_{\mathbf{y}} \mathbf{W}(\mathbf{x},\mathbf{y})$, $\omega_1(\mathbf{y}) = curl_{\mathbf{x}} \mathbf{U}(\mathbf{x}) + curl_{\mathbf{x}} \mathbf{W}(\mathbf{x},\mathbf{y})$, $\mathcal{A}_0 = \nabla_\alpha \mathbf{X}^{(0)} + \nabla_{\mathbf{y}} \mathbf{X}^{(1)}$ is the leading order term in the expansion of the Jacobian matrix of $\mathcal{A}$, and $\langle f \rangle$ stands for averaging of f with respect to $\mathbf{y}$ over one period. It can be shown that $|\mathcal{A}_0| \equiv 1$, which implies the well-posedness of the elliptic equations for the stream functions ψ^0 and ψ^1. Note that equation (29) is a second order elliptic equation for the first order corrector $\psi^{(1)}$ as a function of $\mathbf{y}$ with periodic boundary condition. It plays a similar role as the cell problem for the standard elliptic homogenization. Since the vorticity is of order $1/\epsilon$, it enters the cell problem as a forcing term in the right hand side of the elliptic cell problem. As in elliptic homogenization, we can factor out the slowly varying component $\nabla_\alpha \psi^{(0)}$ from equation (29) for $\psi^{(1)}$. Then we can derive an effective equation for $\psi^{(0)}$ whose effective coefficient is defined through a cell problem that is independent of $\psi^{(0)}$.

The elliptic problems (29)-(30) for $\psi^{(0)}$ and $\psi^{(1)}$ are clearly solvable with appropriate boundary condition. However, to avoid the secular growth of the multiscale expansion, we need to ensure that $\epsilon\mathbf{X}^{(1)} \to 0$ as $\epsilon \to 0$. For this purpose, we need to derive a solvability condition for the $\mathbf{X}^{(1)}$ equation (28).

A solvability condition

As we mentioned above, we need to ensure that $\epsilon\mathbf{X}^{(1)}(\cdot,\cdot,\frac{\alpha}{\epsilon},\frac{t}{\epsilon}) \to 0$ as $\epsilon \to 0$. Let $\mathbf{w} = \nabla_{\mathbf{y}}^\perp \psi^{(1)}$ be the cell velocity, and $\mathbf{Y}(\mathbf{y},\tau)$ be the cell characteristic, i.e. for each α and t fixed, $\mathbf{Y}(\mathbf{y},\tau)$ satisfies

$$\frac{d\mathbf{Y}}{d\tau} = \mathbf{w}(\mathbf{Y},\tau)\ , \quad \mathbf{Y}(\mathbf{y},0) = \mathbf{y}.$$

We decompose the cell velocity field into two parts:

$$\mathbf{w}(t,\alpha,\tau,\mathbf{y}) = \mathbf{w}_1(t,\alpha,\tau,\mathbf{y}) + \mathbf{w}_2(t,\alpha,\tau,\mathbf{y}).$$

To avoid the secular growth term, we need to remove the non-mixable part of the cell velocity, $\mathbf{w}_2$, which corresponds to

$$\lim_{T\to\infty}\frac{1}{T}\int_0^T \mathbf{w}_2(t,\alpha,\tau,\mathbf{Y}(\mathbf{y},\tau))d\tau \to \eta(t,\alpha,\mathbf{y}) \neq 0\ .$$

In another word, we will use the following projection method for $\mathbf{w}$:

$$\mathbf{w}(t,\alpha,\tau,\mathbf{y}) \quad \leftarrow \quad \mathbf{w}(t,\alpha,\tau,\mathbf{y}) - \lim_{T\to\infty}\frac{1}{T}\int_0^T \mathbf{w}(t,\alpha,\tau,\mathbf{Y}(\mathbf{y},\tau))d\tau\ .$$

For the Navier-Stokes equations, viscosity and random forcing play the role to eliminate the non-mixable component of the flow velocity. Eliminating this non-mixable component is essential for the flow to be fully mixed, and to reveal certain universality and scale similarity. For inviscid Euler equations without external forcing, the projection method provides a systematic way to eliminate the non-mixable component. It can be also viewed as an acceleration method for the flow to be fully mixed.

4.2 Multiscale analysis in the Eulerian frame

For computational purpose, it is more convenient to derive a homogenized equation in the Eulerian formulation. As we see from the multiscale analysis in the Lagrangian frame, the key is to introduce a new phase variable, $\theta^\epsilon(t,\mathbf{x})$, to characterize the propagation of the small scales in the fluid flow. This phase variable is convected by the full flow velocity. The multiscale structure of the solution becomes apparent using this new variable. In deriving the multiscale analysis in the Eulerian frame, we use the new phase variable to describe the propagation of the small scale component of the velocity field, but use the Eulerian variable to describe the large scale averaged solution.

One advantage of this approach is that we can characterize the nonlinear convection of small scales exactly using this phase variable and turn a convection dominated transport problem into an elliptic problem for the pressure. Thus, our multiscale finite element methods for elliptic problems described earlier can be used to obtain a multiscale approximation for the small scale pressure equation.

Guided by our multiscale analysis in the Lagrangian frame, we look for multiscale expansions of the velocity field and the pressure of the following form:

$$\mathbf{u}^\epsilon(t,\mathbf{x}) = \mathbf{u}(t,\mathbf{x}) + \mathbf{w}(t,\mathbf{x},\tau,\mathbf{y}) + \epsilon\mathbf{u}^{(1)}(t,\mathbf{x},\tau,\mathbf{y}) + \epsilon^2\mathbf{u}^{(2)}(t,\mathbf{x},\tau,\mathbf{y})\cdots, \quad (31)$$

$$p^\epsilon(t,\mathbf{x}) = p(t,\mathbf{x}) + q(t,\mathbf{x},\tau,\mathbf{y}) + \epsilon p^{(1)}(t,\mathbf{x},\tau,\mathbf{y}) + \epsilon^2 p^{(2)}(t,\mathbf{x},\tau,\mathbf{y})\cdots, \quad (32)$$

where $\tau = t/\epsilon$ and $\mathbf{y} = \theta^\epsilon(t,\mathbf{x})/\epsilon$. We assume that $\mathbf{w}$, and q have zero mean with respect to $\mathbf{y}$ and τ. Note that we do not assume that $\mathbf{w}$ and q are periodic in τ. The phase function θ^ϵ satisfies the following evolution equation:

$$\theta^\epsilon_t + \mathbf{u}^\epsilon\cdot\nabla\theta^\epsilon = \mathbf{0}, \quad \theta^\epsilon(0,\mathbf{x}) = \mathbf{x}. \quad (33)$$

Based on the multiscale analysis in the Lagrangian frame, we can show that θ^ϵ has the following multiscale expansion:

$$\theta^\epsilon = \theta(t, \mathbf{x}) + \epsilon\theta^{(1)}(t, \mathbf{x}, \tau, \frac{\theta^\epsilon}{\epsilon}) + \cdots. \tag{34}$$

It is important that the multiscale expansion for θ^ϵ is defined implicitly. If one tries to expand θ^ϵ as a function of $\mathbf{x}/\epsilon$ and t/ϵ as in (23), one will not be able to obtain a well-posed cell problem.

Expanding the Jacobian matrix, we get $\nabla_x\theta^\epsilon = \mathcal{B}^{(0)} + \epsilon\mathcal{B}^{(1)} + \cdots$. Substituting the expansion into the Euler equation and matching the terms of the same order, we obtain

$$\epsilon^{-1}: \quad \partial_\tau \mathbf{w} + {\mathcal{B}^{(0)}}^\top \nabla_y q = \mathbf{0}, \tag{35}$$

$$\epsilon^0 \quad : \quad \partial_\tau \mathbf{u}^{(1)} + {\mathcal{B}^{(0)}}^\top \nabla_y p^{(1)} =$$
$$-\Big(\partial_t(\mathbf{u}+\mathbf{w}) + ((\mathbf{u}+\mathbf{w})\cdot\nabla_x(\mathbf{u}+\mathbf{w}) + \nabla_x(p+q) + {\mathcal{B}^{(1)}}^\top \nabla_y q\Big) \ , \tag{36}$$

where ${\mathcal{B}^{(0)}}^\top$ stands for the transpose of $\mathcal{B}^{(0)}$.

Further, we note that a necessary condition for the solvability of $\mathbf{u}^{(1)}$ is that the right hand side of (36) has zero mean in with respect to $\mathbf{y}$ and τ. Since $\mathbf{w}$ and q have zero mean in $\mathbf{y}$ and τ, we obtain the following homogenized equation for $\mathbf{u}$ by averaging the right hand side of (36) with respect to $\mathbf{y}$ and τ,

$$\partial_t \mathbf{u} + \mathbf{u}\cdot\nabla_x\mathbf{u} + \langle(\mathbf{w}\cdot\nabla_x)\mathbf{w}\rangle^* + \langle{\mathcal{B}^{(1)}}^\top \nabla_y q\rangle^* = -\nabla_x p, \tag{37}$$

where $\langle f\rangle^*$ stands for average of variable f with respect to $\mathbf{y}$ and τ. Moreover, we can show by using the weak formulation of the Euler equation and the multiscale expansions of $\mathbf{u}^\epsilon$ and p^ϵ that $\langle{\mathcal{B}^{(1)}}^\top \nabla_y q\rangle^* = \langle\mathbf{w}\nabla_x\cdot\mathbf{w}\rangle^*$. Thus the effective equation for $\mathbf{u}$ becomes

$$\partial_t \mathbf{u} + \mathbf{u}\cdot\nabla_x\mathbf{u} + \nabla_x\cdot\langle\mathbf{w}\mathbf{w}\rangle^* = -\nabla_x p, \quad \mathbf{u}|_{t=0} = \mathbf{U}(\mathbf{x}) \ , \tag{38}$$

$$\nabla\cdot\mathbf{u} = 0. \tag{39}$$

where $\mathbf{w}\mathbf{w}$ is a matrix with entry in the ith row and jth column equal to $w_i w_j$.

We remark that it is essential to combine the multiscale analysis in the strong form with the weak formulation of the Euler equation in order to derive a closed homogenized equation. The reason is because we allow multiscale structure in θ^ϵ within the multiscale expansion of the velocity field. If we consider only coefficient equations derived by substituting the multiscale expansions into the Euler equation and matching each order of ϵ, we will lose certain important conservative properties of the original Euler equation. We will not be able to derive a closed set of homogenized equations. In some sense, the weak formulation provides us with additional information that complements the multiscale analysis using asymptotic expansions.

The equation for the small scale velocity field $\mathbf{w}$ is given by (35):

$$\partial_\tau \mathbf{w} + {\mathcal{B}^{(0)}}^\top \nabla_y q = 0, \quad \tau > 0; \tag{40}$$

$$({\mathcal{B}^{(0)}}^\top \nabla_y)\cdot\mathbf{w} = 0, \quad \mathbf{w}|_{\tau=0} = \mathbf{W}(\mathbf{x}, \mathbf{y}). \tag{41}$$

Moreover, it can be shown that ${\mathcal{B}^{(0)}}^\top \nabla_y q$ has zero mean in $\mathbf{y}$ and τ respectively. This guarantees the existence of a periodic solution for $\mathbf{w}$. Moreover, $\mathbf{w}$ will be bounded for large τ since ${\mathcal{B}^{(0)}}^\top \nabla_y q$ has zero mean in τ.

Further, we can derive the evolution equations for θ and $\theta^{(1)}$ as follows

$$\partial_t \theta + (\mathbf{u} \cdot \nabla_x)\theta = \mathbf{0}, \quad \theta|_{t=0} = \mathbf{x}, \tag{42}$$

and

$$\partial_\tau \theta^{(1)} + (\mathbf{w} \cdot \nabla_x)\theta = 0, \quad \theta^{(1)}|_{\tau=0} = \mathbf{0}. \tag{43}$$

From θ and $\theta^{(1)}$, we can compute the Jacobian matrix $\mathcal{B}^{(0)}$ as follows:

$$\mathcal{B}^{(0)} = (I - D_y \theta^{(1)})^{-1} \nabla_x \theta \ . \tag{44}$$

As in the Lagrangian case, we also need to impose a solvability condition for $\theta^{(1)}$. The condition is the same as before, i.e. the τ-average of the cell velocity $\mathbf{w}$ must be zero in order for $\epsilon\theta^{(1)} \to 0$ as $\epsilon \to 0$ (recall $\tau = t/\epsilon$). For this reason, we must project the non-mixable part of the cell velocity to zero, i.e. we apply a projection on $\mathbf{w}$ to filter out the component of $\mathbf{w}$ that has nonzero mean in τ:

$$\mathbf{w} \ \leftarrow \ \mathbf{w} - \lim_{T\to\infty} \frac{1}{T} \int_0^T \mathbf{w} \ d\tau.$$

In practice, this projection step can be carried out locally when we integrate the equation from $t_n = n\Delta t$ to $t_{n+1} = (n+1)\Delta t$, with Δt being the coarse grid time step. In this case, the time average window width T should be set to $T = \Delta t/\epsilon$.

The equation for the first order correction, $\mathbf{u}^{(1)}$, is given by satisfying the Euler equation to $O(1)$

$$\partial_\tau \mathbf{u}^{(1)} + {\mathcal{B}^{(0)}}^\top \nabla_y p^{(1)} = -\left(\partial_t(\mathbf{u}+\mathbf{w}) + ((\mathbf{u}+\mathbf{w})\cdot\nabla_x(\mathbf{u}+\mathbf{w}) + \nabla_x(p+q) + {\mathcal{B}^{(1)}}^\top \nabla_y q\right) \ ,$$
$$\mathbf{u}^{(1)}|_{\tau=0} = \mathbf{0} \ ,$$
$$({\mathcal{B}^{(0)}}^\top \nabla_y)\cdot \mathbf{u}^{(1)} = -\nabla_x \cdot \mathbf{w} - ({\mathcal{B}^{(1)}}^\top \nabla_y)\cdot \mathbf{w}$$

We have used the necessary condition for the solvability of $\mathbf{u}^{(1)}$ to derive the homogenized equation for $\mathbf{u}$. If $\mathbf{u}^{(1)}$ exists and remains bounded, then it will not affect the homogenized equation for $\mathbf{u}$ and the cell problem for $\mathbf{w}$. To establish the convergence of the multiscale expansion, we need to justify that $\epsilon\mathbf{u}^{(1)} \to 0$ as $\epsilon \to 0$. It is easier to study this issue by transforming the problem into the Lagrangian frame. In the Lagrangian frame, the coefficients in the multiscale expansion of the stream function are governed by elliptic equations (see (29)-(30)), whose solvability can be analyzed more easily. The velocity field in the Eulerian frame can be expressed in terms of the Lagrangian stream function and the flow map. The solvability condition for $\mathbf{u}^{(1)}$ can be derived from the corresponding cell problem for the second order correction of the flow map, $\mathbf{X}^{(2)}$.

The above multiscale analysis can be generalized to problems with general multiscale initial data without scale separation and periodic structure. In fact, we

have recently developing a multiscale analysis for the incompressible Euler equation with an infinitely number of scales that are not separable [32]. For initial velocity that has an infinite number of scales, the Fourier coefficients of the initial velocity must satisfy certain decaying property in order to have a bounded energy. We make only a very mild decay assumption in the Fourier spectrum of the initial velocity field, i.e. $|\hat{\mathbf{u}}_k| \leq C|k|^{-(1+\delta)}$ for large $|k|$, where δ is a small positive coefficient. This decay property is consistent with the Kolmogorov spectrum in the inertial range. The analysis developed for the two-scale velocity field provides us with the critical guideline for this more difficult case.

Another way to generalize the above multiscale analysis for problems with many scales is to develop the discrete homogenization analysis. Let H denote the coarse grid mesh size, and h denote the fine grid mesh size. The discrete homogenization is to derive a coarse grid equation that captures correctly the large scale behavior of the well-resolved solution at the fine mesh. By setting ϵ to H, and rescaling the subgrid cell problem by H, we can formally decompose the discrete solution into a large scale component plus a subgrid scale component. The large scale solution corresponds to the "numerically homogenized" solution, and the local fine grid problem corresponds to the small scale cell problem represented by the fine grid solution within each coarse grid block. We can carry out a similar multiscale analysis as before and derive essentially the same set of effective equations. Instead of using periodic boundary condition for $\mathbf{w}$ and q as a function of $\mathbf{y}$, we need to develop a microscopic boundary condition at the boundary of a coarse grid block. Since the cell problem is elliptic, we can apply the over-sampling technique to alleviate the difficulty associated with numerical boundary layer near the edge of the coarse grid block.

We are currently performing careful numerical study to validate our multiscale analysis by comparing the large scale solution obtained by our homogenized equations with that from a well-resolved direct numerical simulation. An important feature of the resulting cell problem for $\mathbf{w}$ is that there is no convection in the fast variable because we treat convection exactly by using the new phase variable. Therefore we can use relatively large time step in τ when we solve the cell problem. Efficient elliptic solver such as multigrid method [53] can be used to solve the cell problem at each time step. Moreover, when the flow is fully mixed, we expect that the space average of the Reynolds stress term, i.e. $\langle \mathbf{ww} \rangle$, will reach to a statistical equilibrium relatively fast in time. As a consequence, we may need to solve for the cell problem in τ for only a small number of fast time steps to obtain the space-time average of the Reynolds stress term, $\langle \mathbf{ww} \rangle^*$. Moreover, we may express the Reynolds stress term as the product of an eddy diffusivity and the deformation tensor of the averaged velocity field, as in the large eddy simulation models [45, 36, 12, 25]. For fully mixed homogeneous flow, the eddy diffusivity is supposed to be a constant in space. In this case, we need only to solve one representative cell problem and use the solution of this representative cell problem to evaluate the eddy diffusivity. This would give a self-consistent coarse grid model that couples the evolution of the small and large scales dynamically.

Bibliography

[1] J. Aarnes and T. Y. Hou, *An efficient domain decomposition preconditioner for multiscale elliptic problems with high aspect ratios,* Acta Mathematicae Applicatae Sinica, **18** (2002), 63-76.

[2] T. Arbogast, *Numerical subgrid upscaling of two-phase flow in porous media,* in Numerical treatment of multiphase flows in porous media, Z. Chen et al., eds., Lecture Notes in Physics 552, Springer, Berlin, 2000, pp. 35-49.

[3] I. Babuska, G. Caloz, and J. E. Osborn, *Special finite element methods for a class of second order elliptic problems with rough coefficients,* SIAM J. Numer. Anal., **31** (1994), 945-981.

[4] A. Bensoussan, J. L. Lions, and G. Papanicolaou, *Asymptotic analysis for periodic structures,* Volume 5 of Studies in Mathematics and Its Applications, North-Holland Publ., 1978.

[5] A. Bourgeat, *Homogenized behavior of two-phase flows in naturally fractured reservoirs with uniform fractures distribution,* Comp. Meth. Appl. Mech. Engrg, **47** (1984), 205-216.

[6] F. Brezzi and A. Russo, *Choosing bubbles for advection-diffusion problems*, Math. Models Methods Appl. Sci., bf 4 (1994), 571-587.

[7] F. Brezzi, L. P. Franca, T. J. R. Hughes and A. Russo, $b = \int g$, Comput. Methods in Appl. Mech. and Engrg., **145** (1997), 329-339.

[8] L. Q. Cao, J. Z. Cui, and D. C. Zhu, *Multiscale asymptotic analysis and numerical simulation for the second order Helmholtz equations with rapidly oscillating coefficients over general convex domains,* SIAM J Numer Anal. (2002), **40**, 543-577.

[9] Z. Chen and T. Y. Hou, *A mixed finite element method for elliptic problems with rapidly oscillating coefficients,* Math. Comput., **72**, No. 242, pp. 541-576, published electronically on June 28, 2002.

[10] J. R. Chen and J. Z. Cui, *A multiscale rectangular element method for elliptic problems with entirely small periodic coefficients,* Applied Math. Comput. (2002), **30**, 39-52.

[11] . Chorin and J. Marsden, **A Mathematical Introduction to Fluid Mechanics,** Second ed., Springer-Verlag, New York, 1984.

[12] R. Clark, J. H. Ferziger, and W. Reynolds, *Evaluation of subgrid-scale models using an accurately simulated turbulent flow,* J. Fluid Mech., **91** (1979), 1-16.

[13] M. Dorobantu and B. Engquist, *Wavelet-based Numerical Homogenization,* SIAM J.Numer. Anal., **35** (1998), 540-559.

[14] J. Douglas, Jr. and T.F. Russell, *Numerical methods for convection-dominated diffusion problem based on combining the method of characteristics with finite element or finite difference procedures,* SIAM J. Numer. Anal. **19** (1982), 871–885.

[15] L. J. Durlofsky, *Numerical calculation of equivalent grid block permeability tensors for heterogeneous porous media,* Water Resour. Res., **27** (1991), 699-708.

[16] L.J. Durlofsky, R.C. Jones, and W.J. Milliken, *A nonuniform coarsening approach for the scale-up of displacement processes in heterogeneous porous media,* Adv. Water Resources, **20** (1997), 335–347.

[17] W. E and T. Y. Hou, *Homogenization and convergence of the vortex method for 2-D Euler equations with oscillatory vorticity fields,* Comm. Pure and Appl. Math., **43** (1990), 821-855.

[18] Y. R. Efendiev, *Multiscale finite element method (MsFEM) and its applications*, Ph. D. Thesis, Applied Mathematics, Caltech, 1999.

[19] Y. R. Efendiev, L. J. Durlofsky, S. H. Lee, *Modeling of subgrid effects in coarse-scale simulations of transport in heterogeneous porous media,* WATER RESOUR RES, **36** (2000), 2031-2041.

[20] Y. R. Efendiev, T. Y. Hou, and X. H. Wu, *Convergence of a nonconforming multiscale finite element method,* SIAM J. Numer. Anal., **37** (2000), 888-910.

[21] W. E and B. Engquist, *The heterogeneous multi-scale method for homogenization problems*, preprint, 2003, submitted to Multiscale Modeling and Simulation.

[22] A. Fannjiang and G. Papanicolaou, *Convection enhanced diffusion,* SIAM J. Appl. Math. **54** (1994), 333-408.

[23] A. Fannjiang and G. Papanicolaou, *Diffusion in turbulence,* Probab. Theor Relat. Fields, **105** (1996), 279-334.

[24] C. W. Gear, I. G. Kevrekidis, and C. Theodoropoulos, *'Coarse' integration/bifurcation analysis via microscopic simulators: micro-Galerkin methods,* Comput. & Chem Eng. (2002), **26**, 941-963.

[25] M. Germano, U. Pimomelli, P. Moin, and W. Cabot, *A dynamic subgrid-scale eddy viscosity model*, Phys. Fluids A (1991), **3**, 1760-1765.

[26] J. Glimm, H. Kim, D. Sharp, and T. Wallstrom, *A stochastic analysis of the scale up problem for flow in porous media,* Comput. Appl. Math., **17** (1998), 67-79.

[27] T. Y. Hou and X. H. Wu, *A multiscale finite element method for elliptic problems in composite materials and porous media,* J. Comput. Phys., **134** (1997), 169-189.

[28] T. Y. Hou, X. H. Wu, and Z. Cai, *Convergence of a multiscale finite element method for elliptic problems with rapidly oscillating coefficients,* Math. Comput., **68** (1999), 913-943.

[29] T. Y. Hou and X. H. Wu, *A multiscale finite element method for PDEs with oscillatory coefficients,* Proceedings of 13th GAMM-Seminar Kiel on Numerical Treatment of Multi-Scale Problems, Jan 24-26, 1997, Notes on Numerical Fluid Mechanics, Vol. 70, ed. by W. Hackbusch and G. Wittum, Vieweg-Verlag, 58-69, 1999.

[30] T. Y. Hou and D.-P. Yang, *Multiscale analysis for three-dimensional incompressible euler equations,* in preparation, 2003.

[31] T. Y. Hou and D.-P. Yang, *Multiscale analysis for convection dominated transport,* in preparation, 2003.

[32] T. Y. Hou and D.-P. Yang, *Multiscale analysis for incompressible flow with infinite number of scales,* in preparation, 2003.

[33] T. J. R. Hughes, *Multiscale phenomena: Green's functions, the Dirichlet-to-Neumann formulation, subgrid scale models, bubbles and the origins of stabilized methods,* Comput. Methods Appl. Mech Engrg., **127** (1995), 387-401.

[34] P. Jenny, S. H. Lee, and H. Tchelepi, *Multi-scale finite volume method for elliptic problems in subsurface flow simulation,* to appear in J. Comput. Phys., 2003.

[35] P. Langlo and M.S. Espedal, *Macrodispersion for two-phase, immiscible flow in porous media,* Adv. Water Resources **17** (1994), 297–316.

[36] A. Leonard, *Energy cascade in large eddy simulation of turbulent flows*, Adv. in Geophysics, **18**A (1974), 237-248.

[37] A. M. Matache, I. Babuska, and C. Schwab, *Generalized p-FEM in homogenization,* Numer. Math. **86**(2000), 319-375.

[38] A. M. Matache and C. Schwab, *Homogenization via p-FEM for problems with microstructure,* Appl. Numer. Math. **33** (2000), 43-59.

[39] D. W. McLaughlin, G. C. Papanicolaou, and O. Pironneau, *Convection of microstructure and related problems,* SIAM J. Applied Math, **45** (1985), 780-797.

[40] F. Santosa and M. Vogelius, *First-order corrections to the homogenized eigenvalues of a periodic composite medium,* SIAM J. Appl. Math, **53** (1993), 1636-1668.

[41] S. Moskow and M. Vogelius, *First order corrections to the homogenized eigenvalues of a periodic composite medium: a convergence proof,* Proc. Roy. Soc. Edinburgh, A, **127** (1997), 1263-1299.

[42] P. Park, *Multiscale numerical methods for the singularly perturbed convection-diffusion equation,* Ph.D. Thesis, Applied Mathematics, Caltech, 2001.

[43] O. Pironneau, *On the Transport-diffusion Algorithm and its Application to the Navier-Stokes Equations*, Numer. Math. **38** (1982), 309–332.

[44] G. Sangalli, *Capturing small scales in elliptic problems using a residual-free bubbles finite element method,* to appear in Multiscale Modeling and Simulation.

[45] J. Smogorinsky, *General circulation experiments with the primitive equations,* Mon. Weather Review, **91** (1963), 99-164.

[46] L. Tartar, *Nonlocal effects induced by homogenization,* in PDE and Calculus of Variations, ed by F. Culumbini, et al, Birkhäuser, Boston, 925-938, 1989.

[47] S. Verdiere and M.H. Vignal,*Numerical and theoretical study of a dual mesh method using finite volume schemes for two-phase flow problems in porous media,* Numer. Math. **80** (1998), 601–639.

[48] T. Wallstrom, S. Hou, M. A. Christie, L. J. Durlofsky, and D. Sharp, *Accurate scale up of two-phase flow using renormalization and nonuniform coarsening*, Computational Geoscience, **3** (1999), 69-87.

[49] T. C. Wallstrom, M. A. Christie, L. J. Durlofsky, and D. H. Sharp, *Application of effective flux boundary conditions to two-phase upscaling in porous media,* Transport in Porous Media, **46** (2002), 155-178.

[50] A. Westhead, *Upscaling the two-phase flow in heterogeneous porous media,* Ph. D. Thesis in progress, Applied Mathematics, Caltech, 2003.

[51] X.H. Wu, Y. Efendiev, and T. Y. Hou, *Analysis of upscaling absolute permeability,* Discrete and Continuous Dynamical Systems, Series B, **2** (2002), 185-204.

[52] Y. Zhang and X.-H. Wu, *A Petrov-Galerkin multiscale finite element method,* preprint, 2000, unpublished.

[53] P. M. De Zeeuw, *Matrix-dependent prolongation and restrictions in a black-box multigrid solver,* J. Comput. Applied Math, **33**(1990), 1-27.